Upper limits on gravitational wave bursts radiated from stellar-core collapses in our Galaxy

Masaki Ando[†], Tomomi Akutsu[‖], Tomotada Akutsu[§], Koji Arai[‡], Youichi Aso[†], Mitsuhiro Fukushima[‡], Kazuhiro Hayama[‡], Nobuyuki Kanda[¶], Kazuhiro Kondo[‖], Norikatsu Mio[+], Shinji Miyoki[‖], Shigenori Moriwaki[+], Shigeo Nagano[‡], Shuichi Sato[‡], Masaru Shibata[a], Hideyuki Tagoshi[*], Hirotaka Takahashi [♯], Ryutaro Takahashi[‡], Daisuke Tatsumi[‡], Yoshiki Tsunesada[‡], Toshitaka Yamazaki[‡], and the TAMA collaboration

[†] Department of Physics, The University of Tokyo, Bunkyo-ku, Tokyo 113-0033, Japan

[‡] National Astronomical Observatory, Mitaka, Tokyo 181-8588, Japan

[§] Department of Astronomy, The University of Tokyo, Bunkyo-ku, Tokyo 113-0033, Japan

[‖] Institute for Cosmic Ray Research, The University of Tokyo, Kashiwa, Chiba 277-8582, Japan

[¶] Graduate School of Science, Osaka City University, Sumiyoshi-ku, Osaka 558-8585, Japan

[+] Department of Advanced Materials Science, The University of Tokyo, Kashiwa, Chiba 277-8561, Japan

[*] Graduate School of Science, Osaka University, Toyonaka, Osaka 560-0043, Japan

[♯] Faculty of Science, Niigata University, Niigata, Niigata 950-2102, Japan

[a] Graduate School of Arts and Sciences, The University of Tokyo, Meguro-ku, Tokyo 153-8902, Japan

E-mail: ando@granite.phys.s.u-tokyo.ac.jp

Abstract.

We present the results of observations with the TAMA300 gravitational-wave detector, targeting burst signals from stellar-core collapse events. We used an excess-power filter to extract gravitational-wave candidates, and developed two methods to reduce fake events caused by non-stationary noises of the detector. These analysis schemes were applied to real data from the TAMA300 interferometric gravitational wave detector. We compared the data-processed results with those of a Monte-Carlo simulation with an assumed Galactic event-distribution model and with burst waveforms expected from numerical simulations of stellar-core collapses, in order to interpret the event candidates from an astronomical viewpoint. We set an upper limit of 5.0×10^3 events/sec on the burst gravitational-wave event rate in our Galaxy with a confidence level of 90%.

PACS numbers: 04.80.Nn, 07.05.Kf, 95.85.Sz, 95.55.Ym

1. Introduction

Recently, several interferometric gravitational wave (GW) detectors [1, 2, 3, 4, 5] are under operation, and the collected data are being analyzed to search GW signals. In these detectors, which have 100 Hz - 1 kHz observation bands, burst gravitational wave emitted from stellar-core collapse in a supernova explosion is one of the promising targets. However, since GW signals are considered to be faint, an efficient data-analysis scheme is required to extract the signals of GWs from noisy detector outputs. Unlike the chirp, ringdown, and continuous wave cases, a matched filtering method cannot be used in a burst-wave analysis because a set of precise waveform templates that cover the source parameters is not available. Thus, several signal-extraction methods, called 'burst filters', have been proposed for the detection of these burst gravitational waves: an excess power filter [6], a cluster filter in the time-frequency plane [7], a wavelet-based power filter [8], a slope (or a linear-fit) filter [9], and a pulse correlation filter [10]. Since we have only a little knowledge on the waveforms, these filters look for unusual events in the Gaussian-noise background.

For the detection of GWs, the evaluation and reduction of fake-event backgrounds are critical problems. Since burst filters are designed to extract any unusual behavior of the detector output, they are also sensitive to non-stationary noises of the detector. Moreover, it is not straightforward to distinguish these fakes from a real signal, and to reject them, because we do not know the precise GW waveforms. With these fake events, it is likely that real signals are buried in fakes, or are dismissed with a larger detection threshold set to reduce fakes. There are several schemes used to reject these fake events: coincidences by multiple detectors, veto analyses with detector monitor signals, rejection by waveform behaviors, and so on. Among them, the most powerful and reliable way will be a coincidence analysis with multiple independent detectors [11, 12, 13, 14]. If we detect gravitational-wave candidates with multiple detectors simultaneously (or within an acceptable time difference), we can declare the detection of a real signal with high confidence. On the other hand, fake reduction with a single detector [15, 16, 17] is also important, even in a coincidence analysis, since the rejection of fakes with a single detector would reduce accidental coincidences.

In this article, we present a data-analysis scheme for burst GWs, and results obtained by applying them to real observation data. The data used in this work were about 200 hours of data collected during the ninth data-taking run (DT9) of the TAMA300 detector [4, 5]. We adopted an excess power filter as a burst filter, which is robust for uncertainties of the GW waveforms [6, 18]. In addition, we used two fake-reduction methods. One was a veto with detector monitor signals. Another was a fake-rejection method based on the waveform behavior of the time scale. The obtained event triggers were interpreted from an astronomical point of view; we intended to set upper limits on Galactic events [11, 18, 19, 20] using a realistic distribution of the Galactic events, targeting realistic waveforms obtained by numerical simulations, and analyzing long observation data from the detector. For this purpose, we carried out Monte-Carlo

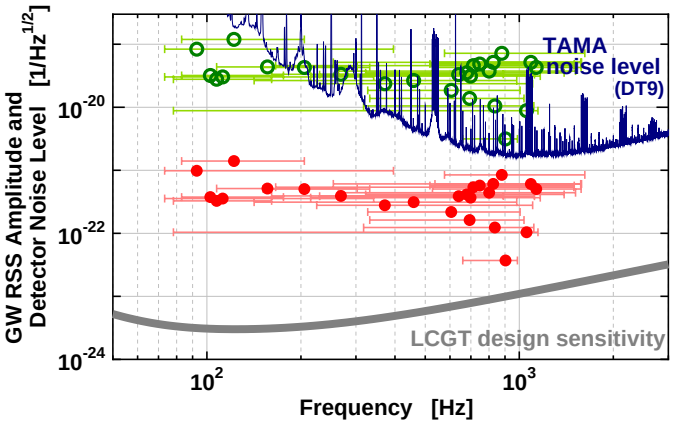

Figure 1. RSS amplitude and central frequency calculated from waveforms in the DFM catalog. The amplitudes are for events at the Galactic center (closed circles), and for events at 100 pc distance from the detector (open circles). The source angle is assumed to be optical in this plot. Each error bar indicates the frequency range within which the power spectrum value is above half of its peak value. The noise level of TAMA at DT9 and the design sensitivity of LCGT [28] are shown together.

simulations of Galactic events with waveforms obtained by numerical simulations of stellar-core collapses.

2. Generation of event triggers: target waveforms, used data, and schemes

2.1. Target gravitational waves

The target of the analysis in this work is a burst GW from stellar-core collapse (core-collapse supernova explosion). It is difficult to predict its waveform analytically, because of the complex time evolution of the mass densities in the explosion process. Thus, the explosion process and radiated GWs have been investigated by numerical simulations [21, 22, 23]. Although these simulations were performed with differently simplified models, similar waveforms were obtained in these simulations. Among these simulations, Dimmelmeier et al. have presented rather systematic surveys on GWs from stellar-core collapses [21]. They have obtained 26 waveforms with relativistic simulations of rotational supernova core collapses, with axisymmetric models with different initial conditions in a differential rotation, an initial rotation rate, and an adiabatic index at subnuclear densities. Although the simulation did not cover all of the initial parameters, we used them as reference waveforms in our analysis, assuming that typical characteristics and behavior of the GWs from stellar-core collapses are included in this waveform catalog.

We processed the original waveforms of the catalog (we call it DFM catalog in this article) with a 30 Hz second-order high-pass digital filter, and resampled them to 20 kHz in order to be compatible with the data from the detector. According to the DFM catalog, the averaged amplitude of GWs radiated by supernovae at the Galactic

center (8.5 kpc distance from the detector) is $\langle h_{\rm peak} \rangle = 1.5 \times 10^{-20}$ in a peak strain amplitude, or $\langle h_{\rm rss} \rangle = 4 \times 10^{-22}$ [Hz$^{-1/2}$] in root-sum-square (RSS) amplitude [19, 24]. In the axisymmetric model used to obtain the DFM catalog, the waves are radiated only in a plus-polarization, and the radiated amplitude has an angular dependence of $(\sin\theta)^2$, where θ is the angle between the symmetric axis and the propagation axis of GW to the detector [21, 22, 23]. The amplitudes described above are calculated with the optimal source angle ($\theta = \pi/2$). The central frequencies of the waves, which are calculated from the weighting average of the power spectra, range from 90 Hz to 1.2 kHz (Fig. 1), which is around the observation band of interferometric detectors. Also, it is estimated from the DFM catalog that a total energy radiated as GWs in one event is $\langle E_{\rm tot} \rangle = 8 \times 10^{-8}\,[M_\odot c^2]$, in average [21]. Here, $M_\odot$ is the mass of the Sun.

2.2. Data from a gravitational wave detector TAMA300

We used observation data obtained by TAMA300 [4, 5]; TAMA300 is a Japanese laser-interferometric gravitational wave detector, located at the Mitaka campus of the National Astronomical Observatory of Japan (NAOJ) in Tokyo (35°40′N, 139°32′E). TAMA300 has an optical configuration of a Michelson interferometer with 300 m-length Fabry-Perot arm cavities and with power recycling to enhance the laser power in the interferometer. The main output signal of the detector, which would contain GW signals, is recorded with a 20 kHz, 16 bit data-acquisition system [25]. Besides the main output signal, over 150 monitor signals, which are used for diagnosing the detector condition and for veto analyses are also recorded during the observation. The recorded data are stored in DLT tapes on site, and are sent to data-analysis computers at the collaborating institutes by Giga-bit optical network connections.

At TAMA, nine observation runs have been carried out so far since the first observation run in 1999, and over 2700 hours of data have been collected. In the latest observation run, the ninth data-taking run (DT9), we collected over 500 hours of data. In this work, we used 200 hours of data with low noise and uniform quality in the second half of DT9 to obtain the event upper limit. The typical noise spectrum in DT9 is shown in Fig. 1. The floor level is 2×10^{-21} [Hz$^{-1/2}$] in DT9 at around 1 kHz. The spectrum contains several line peaks: harmonics of a 50 Hz AC line, violin-mode peaks (around 520 Hz and integer multiples) of the suspension wire of the mirror, and a calibration peak. Since these lines could affect the analysis results, they were removed in the data analyses.

2.3. Extraction of signals by an excess-power filter

We developed and implemented a burst-wave analysis code based on an excess-power burst filter. An excess-power filter is robust because it uses only a little information on the target waveforms: the signal duration time and the frequency band. The evaluation parameter is the total noise power in a given time-frequency region. In spite of its

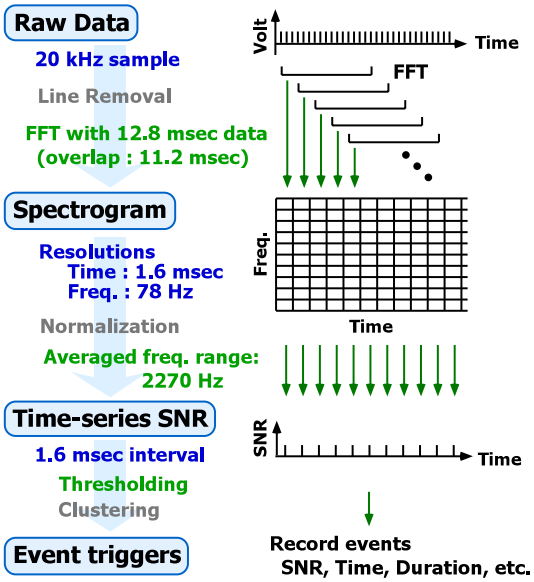

Figure 2. Data-processing chart of our excess-power burst filter. We first calculate a spectrogram from the detector output data. Next, we obtain the time-series SNR by averaging the frequency components. Then, we extract event triggers by a given threshold.

robustness, it is nearly as efficient as matched filtering for signals with short duration and a limited frequency band [6].

Our filter generates event triggers in the following steps (Fig. 2): (i) A spectrogram (time-domain change in noise power spectrum) is calculated from the output data of the detector; the power spectrum is calculated with a $\Delta t = 12.8\,[\mathrm{msec}]$ data segment using a fast Fourier transform (FFT), which is repeated with 1.6 msec time-delays. Lines (AC line peaks in every 50 Hz, etc.) contained in the original data are removed from the original time-series data before calculating the spectrogram. (ii) In each spectrum, power in pre-selected frequency bands is averaged so as to obtain a time-series of the averaged power, P_n. Each spectrum is normalized (whitened) by the typical noise spectrum within 30 min before a calculation of the average in the frequency components. As a result, P_n represents the signal-to-noise ratio (SNR): the ratio of the averaged signal power to the typical noise power in pre-selected time-frequency region. In this work, we selected a fixed band of $\Delta f = 2270\,[\mathrm{Hz}]$ from 230 Hz to 2.5 kHz. (iii) Event triggers are extracted if the averaged power is larger than a given threshold, $P_n \geq P_{\mathrm{th}}$. If unusual signals in the detector output are sufficiently large, they will be observed in the filter output. Continuous excesses above the threshold are clustered to be a single event.

The parameters of the filter, length of the time segment (Δt) for each FFT, and analysis frequency band (Δf) were selected to be effective for the reference burst GW signals. According to the DFM catalog, the signals have short spike-like waveforms, i.e. a short duration and a wide frequency band. Although the selected parameters ($\Delta t = 12.8\,[\mathrm{msec}]$, $\Delta f = 2270\,[\mathrm{Hz}]$) were not fully optimized for the waveforms, the

analysis results were not changed very much with a different parameter set. Moreover, we could keep the robustness of the excess-power filter with this rough tuning of the time-frequency bands.

2.4. Reduction of fake events

We have used two veto methods so as to reject fake events caused by detector instabilities: a veto method using auxiliary signals for the detector monitor, and a veto by the time-scale-selection of the events.

The first veto scheme used in our analysis was a veto method using auxiliary signals recorded together with the main output of the detector. We found strong correlations between the short spikes in the main output and the monitor signal for the laser intensity in a power-recycling cavity of the interferometer. The intensity-monitor data were processed by the same excess-power filter to detect short-spike instabilities. The filter parameters were the same as that for the main signal analysis, except for the frequency range ($\Delta f_{\rm int} = 1170\,{\rm Hz}$). When the outputs of two excess power filters (one for the GW signal-channel, and another for the intensity monitor) exceed the respective thresholds simultaneously, the triggers are labeled as fakes, and are removed from the event candidate list. We confirmed that this veto is safe, in other words that the intensity instabilities were not caused by huge GW signals, by shaking the interferometer mirrors with simulated waveforms [22] of various amplitudes (a 'hardware injection' test). The false-dismissal rate in this veto is equal to the accidental coincidence rate between the intensity excess and the excess in GW signal-channel, which was estimated from the distribution of the power in the intensity monitor signal. We selected a threshold so that the false-dismissal rate would be 1%.

The second veto scheme is a veto by the time-scale of the signal. It is hard to see any clear correlations for all of the fake events in practice, because there are various origins of the fakes, which are difficult to be identified. Thus, a test of the signal behavior at the main output of the detector will be helpful to reduce fake events. The effectiveness of the veto with a signal behavior test depends on how well we know, or how many assumptions we set, on the signal behavior. In the burst-wave analysis case, the waveforms by numerical simulations suggest that GWs from stellar-core collapse have a short duration, typically less than 100 msec. We know that some of the detector instabilities last longer than a few seconds from experience. Thus, some of the fakes caused by these slow instabilities are rejected by evaluating the time scale of the event triggers [17]. The false-dismissal rate was directly evaluated from the results of a signal-injection test with the real data from the TAMA300 detector. As a result, the false-dismissal rate was only 0.08% in the Galactic signal-injection test described in the next section.

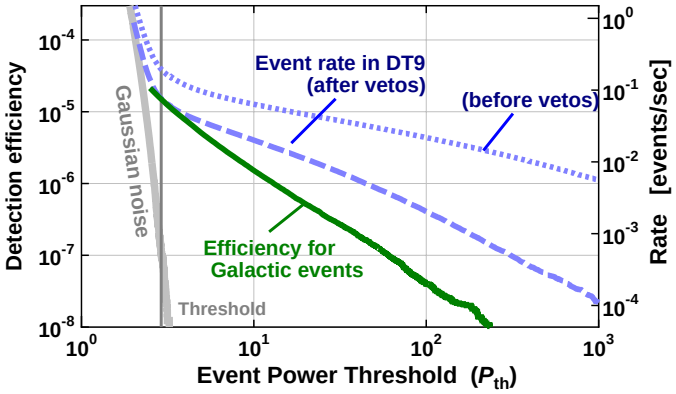

Figure 3. Results of the TAMA observation and a Galactic-event simulation. The solid curve shows the detection efficiency for Galactic events as a function of the threshold. The trigger rate obtained by the DT9 observation is also plotted as dashed (after vetoes) and dotted (before vetoes) curves.

3. Data-processing results with the TAMA300 data

3.1. Event-trigger rates

The analysis method described above was applied to real data from TAMA300. The data were mainly processed by a PC-cluster computer placed at the University of Tokyo. This machine is comprised of 10 nodes, and has 20 CPUs (Athlon MP 2000+ by AMD Inc.). The analysis time for the excess power filter was about 30-times faster than the real time; it took about 1/30 sec to process 1-sec data. In data processing, the first 9-min and the last 1-min data of the each continuous observation span were not used because they sometimes contained loud noises caused by detector instabilities, or excited violin-mode fluctuations. In addition, the duration time of rejected fake events is considered to be a dead time of the detector, and is subtracted from the total observation times. The dead time by the fake rejections was 0.4% of the observation time in DT9. The effective observation time ($T_{\rm obs}$) was 194.6 hours after vetoes.

The dashed line in Fig. 3 shows the event-trigger rates obtained by the TAMA data analyses; the trigger rate (in a unit of events/sec, right axis) is plotted as a function of the event-extraction threshold ($P_{\rm th}$). The analysis result with simulated Gaussian noise is also plotted in Fig. 3. Though the trigger rates were reduced with vetoes, the rates are still much larger than that with simulated Gaussian noises, even with the vetoes. In addition, the trigger rate is still much higher than the expected rate of supernova explosions. The expected GW event rate is one event in a few tens of years, i.e. about 10^{-9} events/sec in our Galaxy. (Here, we note that TAMA has a detectable range of 300 pc for events with the optimal direction and polarization.) These results suggest that most of the observed trigger-events were fake events caused by an instability of the detector, even with vetoes.

3.2. Simulations of Galactic events

We cannot claim the detection of GW signals from the data-analysis results described above because it is difficult to distinguish a real signal from background fake triggers with a single detector. Thus, we set upper limits for stellar-core collapse events in our Galaxy. We carried out Monte-Carlo simulations with a source-distribution model of our Galaxy, and with waveforms from the DFM catalog. The simulated data were analyzed in the same way as the detector data, and compared with the observation results.

In the simulation, we adopted a source-distribution model based on the observed luminous star distribution in our Galaxy, assuming that the event distribution of the stellar-core collapses was identical to it. In our simulation, we used a simple axisymmetric distribution model (an exponential disk model) described in a cylindrical coordinate,

$$\rho(R, \varphi, z) \propto \exp\left(-\frac{R}{R_0} - \frac{|z|}{h_0}\right), \tag{1}$$

where ρ, $R_0 = 3.5\,\mathrm{kpc}$, and $h_0 = 325\,\mathrm{pc}$ are the density of the events, and the characteristic radius and height of the density of the Galactic disk, respectively [26, 27]. As well as the non-axisymmetric components, such as spiral arms, the thick disk and halo structures were neglected in our simulations because their number of stars was only about 3% of that of the disk component [27]. We adopted $R_\odot = 8.5\,\mathrm{kpc}$ and $h_\odot = 20\,\mathrm{pc}$ for the position of the Sun in our simulation.

This test was performed according to the following steps: (i) Set the GPS times at which simulated events are injected; these times are uniformly separated between the start and end times of the observation run. Decide the position of each event randomly according to the Galactic-event distribution described by Eq. (1). (ii) Select the waveform of each event randomly from the DFM catalog. The orientation of the source symmetric axis was selected to be random: $\rho(\theta, \psi) = \sin\theta/2$, where θ and ψ are the angle between the symmetric axis and the propagation axis of GW to the detector, and the rotation angle around the propagation axis, respectively. (iii) The expected GW amplitude is calculated from the distance to the event source, the detector antenna pattern for the sky position of the event, and the orientation of the symmetric axis and polarization of the source. (iv) Inject each event waveform to the TAMA300 data with estimated amplitude, and analyze the data with the same code as that for the raw-data analysis. (v) Extract the events at the injected time.

3.3. Results of Galactic-event simulations

Figure 3 shows the results of a Galactic-event simulation. The fraction of detectable Galactic events (the detection efficiency, ϵ_{gal}, left axis) is plotted as a function of the SNR threshold (P_{th}). With an event-selection threshold of $P_{\mathrm{th}} = 2.9$ (which corresponds to averaged amplitude of $h_{\mathrm{rss,th}} = 1.6 \times 10^{-20}\,[\mathrm{Hz}^{-1/2}]$ for DT9), the detection efficiency was estimated to be $\epsilon_{\mathrm{gal}} = 1.5 \times 10^{-5}$ for the Galactic events. The threshold was selected so that the expected contribution of the Gaussian noise would be sufficiently

small (less than 1% of the triggers above the threshold). The upper limit for the event rate determined from the TAMA raw-data was $R_{\rm DT9,UL} = 7.5 \times 10^{-2}$ [events/sec] with a confidence level of 90%. We obtained this upper limit using Bayesian statistics with uniform prior probability, and assuming the Poisson distribution for the number of real events. From these results, we obtained the upper limit for the Galactic event rate to be $R_{\rm gal,UL} = R_{\rm DT9,UL}/\epsilon_{\rm gal} = 5.0 \times 10^3$ [events/sec] with a 90% confidence level. This value is considerably larger than the theoretical expectation of about 10^{-9} events/sec.

Besides the upper limit for the rate of a stellar-core collapse in our Galaxy, an upper limit was set for the GW energy rate. The total energy radiated as GW, $E_{\rm tot}$, was estimated for each event from its waveform. The upper limit for the energy rate radiated as GW was estimated by the product of the event-rate upper limit, $R_{\rm gal,UL}$, and the averaged GW energy of the events, $\langle E_{\rm tot} \rangle$. As a result, we obtained $\dot{E}_{\rm GW,UL} = 4.4 \times 10^{-4}\,[M_\odot c^2/{\rm sec}]$. Again, this value is considerably large; the rate of the total energy radiated as GWs would be about $M_{\rm Gal}/(1.4 \times 10^7)\,[M_\odot c^2/{\rm years}]$, where $M_{\rm Gal}$ is the total mass of our Galaxy, which we assume to be $2 \times 10^{11}\,M_\odot$.

4. Conclusion

We presented data-analysis schemes and results of observation data by TAMA300, targeting at burst signals from stellar-core collapses. Since precise waveforms are not available for burst gravitational waves, the detection schemes (the construction of a detection filter and the rejection of fake events) are different from those for chirp wave analyses. We investigated two methods for the reduction of non-stationary noises, and applied them to real data from the TAMA300 interferometric gravitational wave detector. The fake-event rate was reduced by a factor of about 1000 in the best case.

The obtained event-trigger rate was interpreted from the viewpoint of the burst gravitational-wave events in our Galaxy. From the observation and analysis results, we set the upper limit for the Galactic event rate to be 5.0×10^3 events/sec (confidence level 90%), based on a Galactic disk model [27] and waveforms obtained by numerical simulations of stellar-core collapses [21]. In addition, we determined the upper limit for the rate of the energy radiated as gravitational-wave bursts to be $4.4 \times 10^{-4}\,M_\odot c^2$/sec (confidence level 90%). These large upper limits show that the detector output was still dominated by fake events, even after the selection of events, and gives us prospects concerning both current and future research: the necessity for further improvement of the analysis schemes, coincidence analyses with multiple detectors, better predictions on the waveforms, and future detectors, such as LCGT [28] and advanced LIGO [29], to cover the whole of our Galaxy.

Acknowledgments

This research is supported in part by a Grant-in-Aid for Scientific Research on Priority Areas (415) of the Ministry of Education, Culture, Sports, Science and Technology.

References

[1] A. Abramovici *et al.*, Science **256** 325 (1992).

[2] The VIRGO collaboration, *VIRGO Final Design Report* VIR-TRE-1000-13 (1997), C. Bradaschia, *et al.*, Nucl. Instrum. Meth. A **289** 518 (1990).

[3] K. Danzmann *et al.*, *Proposal for a 600m Laser-Interferometric Gravitational Wave Antenna* (Max-Planck-Institut für Quantenoptik Report) 190 (1994).

[4] K. Tsubono, *Gravitational Wave Experiments*, eds: E. Coccia, G. Pizzella, and F. Ronga (World Scientific) p. 112 (1995), K. Kuroda et al., *Gravitational Waves: Sources and Detectors*, eds: I. Ciufolini and F. Fidecaro (World Scientific) p. 100 (1997).

[5] M. Ando *et al.*, Phys. Rev. Lett. **86** 3950 (2001).

[6] W. G. Anderson *et al.*, Phys. Rev. D **63** 042003 (2001), W. G. Anderson *et al.*, Phys. Rev. D **60** 102001 (1999), A. Viceré, Phys. Rev. D **66** 062002 (2002).

[7] S. S. Mohanty, Phys. Rev. D **61** 122002 (2000), J. Sylvestre, Phys. Rev. D **66** 102004 (2002).

[8] S. Klimenko, G. Mitselmakher, Class. Quantum Grav. **21** (2004)S1819.

[9] T. Pradier *et al.*, Phys. Rev. D **63** 042002 (2001), N. Arnaud *et al.*, Phys. Rev. D **67** 062004 (2003).

[10] N. Arnaud *et al.*, Phys. Rev. D **59** 082002 (1999).

[11] D. Nicholson *et al.*, Phys. Lett. A **218** 175 (1996).

[12] H. Takahashi *et al.*, Phys. Rev. D **70** 042003 (2004), N. Arnaud *et al.*, Phys. Rev. D **68** 102001 (2003).

[13] P. Astone *et al.*, Phys. Rev. D **59** 122001 (1999), Z. Allen *et al.*, Phys. Rev. Lett. **85** 5046 (2000), P. Astone *et al.*, Class. Quantum Grav. **11** 2093 (1994).

[14] P. J. Sutton *et al.*, Class. Quantum Grav. **21** S1801 (2004).

[15] L. Cadonati and E. Katsavounidis, Class. Quantum Grav. **20** S633 (2003), K. Kotter *et al.*, Class. Quantum Grav. **20** S895 (2003).

[16] S. D. Mohanty and S. Mukherjee, Class. Quantum Grav. **19** 1471 (2002).

[17] M. Ando *et al.*, Class. Quantum Grav. **20** S697 (2003).

[18] M. Ando *et al.*, Phys. Rev. D submitted (2005).

[19] B. Abbott *et al.*, Phys. Rev. D **69** 102001 (2004).

[20] P. Astone *et al.*, Phys. Rev. D **68** 022001 (2003).

[21] H. Dimmelmeier , J. A. Font, and E. Müller, Astron. Astrophys. **393** 523 (2002).

[22] T. Zwerger and E. Müller, Astron. Astrophys. **317** L79 (1997), E. Müller, M. Rampp, R. Buras, H. Janka, and D. Shoemaker, Astrophysical Journal **603** 221 (2004).

[23] C. D. Ott, A. Burrows, E. Livne, and R. Walder Ap. J. **600** 834 (2004), T. Harada, H. Iguchi, and M. Shibata, Phys. Rev. D **68** 024002 (2003), K. Kotake, S. Yamada, and K. Sato, Phys. Rev. D **68** 044023 (2003), M. Shibata and Y. Sekiguchi, Phys. Rev. D **69** 084024 (2004).

[24] L. Cadonati, Class. Quantum Grav. **21** S1695 (2004).

[25] D. Tatsumi *et al.*, in: *Gravitational Wave detection II*, eds.: S. Kawamura, N. Mio, Universal Academy Press (2000) pp. 113-121.

[26] R. Wainscoat, M. Cohen, K. Volk, H. Walker, and D. Schwartz, Ap. J. S. **83** 111 (1992) and the references therein.

[27] J. Larsen and R. Humphreys, Astronomical Journal **125** 1958 (2003).

[28] K. Kuroda *et al.*, Int. J. Mod. Phys. D **8** 557-579 (1999), K. Kuroda *et al.*, Class. Quantum Grav. **20** S871 (2003).

[29] P. Fritschel, 'Second generation instruments for the Laser Interferometer Gravitational Wave Observatory (LIGO)' in: Proceedings of the SPIE meeting 'Gravitational-Wave Detection' (4856-39), eds: P. Saulson and M. Cruise, pp. 282-291 (Waikoloa, Hawaii, 2002).